

Article

The Impact of Cattaneo–Christov Double Diffusion on Oldroyd-B Fluid Flow over a Stretching Sheet with Thermophoretic Particle Deposition and Relaxation Chemical Reaction

Bheemasandra M. Shankaralingappa ^{1,2}, Ballajja C. Prasannakumara ³, Bijjanal J. Gireesha ¹
and Ioannis E. Sarris ^{4,*} 

¹ Department of Studies and Research in Mathematics, Kuvempu University, Shimoga 577451, India; shankar.gsch@gmail.com (B.M.S.); bjgireesu@gmail.com (B.J.G.)

² Department of Mathematics, Government Science College (Autonomous), Hassan 573201, India

³ Department of Studies and Research in Mathematics, Davangere University, Davangere 577002, India; dr.bcprasanna@gmail.com

⁴ Department of Mechanical Engineering, University of West Attica, 12244 Athens, Greece

* Correspondence: sarris@uniwa.gr; Tel.: +30-694-167-2950



Citation: Shankaralingappa, B.M.; Prasannakumara, B.C.; Gireesha, B.J.; Sarris, I.E. The Impact of Cattaneo–Christov Double Diffusion on Oldroyd-B Fluid Flow over a Stretching Sheet with Thermophoretic Particle Deposition and Relaxation Chemical Reaction. *Inventions* **2021**, *6*, 95. <https://doi.org/10.3390/inventions6040095>

Academic Editors: M.M. Bhatti and Sara I. Abdelsalam

Received: 29 October 2021

Accepted: 23 November 2021

Published: 25 November 2021

Publisher's Note: MDPI stays neutral with regard to jurisdictional claims in published maps and institutional affiliations.



Copyright: © 2021 by the authors. Licensee MDPI, Basel, Switzerland. This article is an open access article distributed under the terms and conditions of the Creative Commons Attribution (CC BY) license (<https://creativecommons.org/licenses/by/4.0/>).

Abstract: The current study focuses on the characteristics of flow, heat, and mass transfer in the context of their applications. There has been a lot of interest in the use of non-Newtonian fluids in biological and technical disciplines. Having such a substantial interest in non-Newtonian fluids, our goal is to explore the flow of Oldroyd-B liquid over a stretching sheet by considering Cattaneo–Christov double diffusion and heat source/sink. Furthermore, the relaxation chemical reaction and thermophoretic particle deposition are considered in the modelling. The equations that represent the indicated flow are changed to ordinary differential equations (ODEs) by choosing relevant similarity variables. The reduced equations are solved using the Runge–Kutta–Fehlberg fourth–fifth order technique (RKF-45) and a shooting scheme. Physical descriptions are strategized and argued using graphical representations to provide a clear understanding of the behaviour of dimensionless parameters on dimensionless velocity, concentration, and temperature profiles. The results reveal that the rising values of the rotation parameter lead to a decline in the fluid velocity. The rise in values of relaxation time parameters of temperature and concentration decreases the thermal and concentration profiles, respectively. The increase in values of the heat source/sink parameter advances the thermal profile. The rise in values of the thermophoretic and chemical reaction rate parameters declines the concentration profile.

Keywords: Oldroyd-B liquid; Cattaneo–Christov double diffusion; stretching sheet; thermophoretic particle deposition; relaxation chemical reaction

1. Introduction

The non-Newtonian liquid concerns in fluid mechanics have attracted the interest of various researchers because of their usage in industry and technology. The flow behaviour of non-Newtonian liquids must be studied in depth to have a thorough grasp of them and their various applications. When it comes to non-Newtonian fluid mechanics, engineers, physicists, and mathematicians face a unique challenge. Due to the complexity of non-Newtonian liquids, no one constitutive equation can account for all of their characteristics. As a consequence, many non-Newtonian liquid models have been presented. In recent years, the Oldroyd-B fluid (OBF), which includes the Maxwell liquid and classical Newtonian liquid as special cases, has risen to a unique place among the many fluids of the rate type. Most polymeric and biological fluids have memory and elastic effects, which are accounted for by an OBF. It has been widely used in many applications, with

simulation results based on a wide range of experimental data. Irfan et al. [1] explained the impact of thermal-solutal stratifications on the stagnation point flow of an OBF. Reddy et al. [2] inspected the flow of fluid models such as Maxwell, Oldroyd-B, and Jeffery with a heat source/sink through a cone. Almakki et al. [3] investigated the entropy formation using Brownian movement and thermophoresis diffusions using Maxwell, Oldroyd-B, and Jeffery nanofluid models. Ramzan et al. [4] showed the MD effect on the flow of a ferromagnetic OBF with melting and activation energy effects. Sarada et al. [5] reviewed the lack of a thermal equilibrium effect on OBF and Jeffrey fluid flow on a stretching sheet.

Due to their many applications in industrial and engineering equipment such as polymer processes, plastics extrusion, heat exchangers, and freezers, researchers are increasingly paying excessive attention to mass and heat transfer studies. The laws of Fourier and Fick are used to explain how heat and mass flow through a medium as a result of temperature and concentration variations. According to Fourier's rule, heat transmission has an unlimited speed and propagates across the medium, which provides a parabolic-type equation for temperature. To solve this heat transport problem, Fourier's law must be tweaked. Cattaneo modified Fourier's law by multiplying the thermal relaxation time parameter by the heat flow time derivative, resulting in a hyperbolic-type equation for heat transport phenomena. As a result, heat transport has a limited speed across the medium. To explain the thermal relaxation factor in heat transport, the Cattaneo–Christov heat flow model was proposed. Hayat et al. [6] explored the impact of Cattaneo–Christov double diffusion on the flow of Walters-B nanofluid on an SS with heat sink/source effects. Gireesha et al. [7] analyzed the effect of a modified Fourier heat flux on a dusty liquid stream on an SS. Sowmya et al. [8] explored the magnetized flow of Williamson nanomaterial liquid on an SS with the non-Fourier heat flux model with Brownian motion and thermophoresis (BMT) effects. Prasannakumara [9] described a flow of Maxwell liquid on a sheet containing suspended nanomaterials with the Cattaneo–Christov heat flow model. Gowda et al. [10] conferred the slip effect on a Casson–Maxwell nanofluid flow on a stretchable disk with double diffusion effects.

The boundary layer flow across a stretching surface (SS) has contracted a lot of interest because of its many applications in engineering, manufacturing, and metallurgy. Heat transfer is critical since it allows for controlling the cooling rates and the production of finished items with desired characteristics. Several studies on the flow of various fluids over an SS with different affecting parameters have been reported in relation to these. Hayat et al. [11] conferred the convective heat transfer in the flow of Walters-B liquid on an SS. Prasannakumara [12] exemplified the local thermal non-equilibrium effect on the stream of nanoliquid on an SS by considering the Tiwari–Das model. Christopher et al. [13] discussed the chemical reaction consequence on the flow of hybrid nanoliquid on an SS with Cattaneo–Christov heat flux. Gowda et al. [14] examined the convective stream of second grade fluid on a coiled SS with Dufour and Soret effects. Alhadhrami et al. [15] pondered the LTNE impact on the flow of Casson liquid on an SS with a porous medium. Recently, Ali et al. [16–20] conferred the flow of different fluids past stretching surfaces with several influencing factors by considering different nanoparticles' suspension.

Particles suspended in a liquid flow may move for a variety of causes. This motion might be caused by viscous drag, Brownian diffusion, inertia, or other body forces. The thermophoretic force is created when suspended particles travel from high heat areas to low thermal regions, and the subsequent particle motion is termed as thermophoresis. The findings of investigations on the deposition of aerosol particles on surfaces have proved valuable in various engineering domains. The thermophoresis phenomenon has a primary role in several fields such as bioengineering [21–23]. Recently, several researchers have discussed the significance of thermophoresis in different nanofluid flows [24–30]. Shehzad et al. [31] inspected the convective flow of Maxwell liquid in a spinning disk by considering the thermophoretic particle deposition (TPD). Kumar et al. [32,33] examined the impact of TPD on indifferent fluid flows' temperature and mass distribution. Chen et al. [34] studied the TPD in Casson liquid flow with general Fourier and Fick's laws. Alhadhrami

et al. [35] swotted the impact of TPD on a Glauert wall jet slip flow in the presence of nanofluid. A chemical reaction has been more critical in studying mass transfer in a variety of engineering processes in recent years. Zang et al. [36] used the Cattaneo–Christov double diffusion model to confer the mass and heat transport in the dissipative flow of an OBF on an SS by using a chemical reaction with relaxation-time characteristics. Mburu et al. [37] used relaxation–retardation viscous dissipation to confer the dissipative flow of an OBF on a surface by using a chemical reaction with relaxation-time characteristics. Khan et al. [38] studied the consequence of a chemical reaction on a viscous liquid stream on a curved SS. Gowda et al. [39] conferred the Marangoni convective flow of liquid on a surface with binary chemical reaction. Yusuf et al. [40] explored the consequence of a chemical reaction on a Williamson fluid stream on an inclined plate.

As per the research mentioned above, numerous researchers have explored the flow, heat, and mass transfer in Oldroyd-B liquid flow through the linearly stretching sheet and solved the governing equations using various analytical approaches. We noticed that no previous research had addressed the topic after conducting a comprehensive examination of the literature. This investigation considers the linearly stretching sheet since it has numerous applications in the plastic and metal extrusion industries. According to the preceding literature review, no numerical solution for the given flow has ever been investigated. This research gap motivated us to investigate the impact of effective factors on the flow features of an OBF on the SS using the RKF-45 method. Thus, the main goal of this study is to examine the three-dimensional incompressible steady Oldroyd-B flow over a linearly stretching sheet by using the Cattaneo–Christov theory and thermophoretic particle deposition. Furthermore, the graphs are also used to discuss the variations in detailed profiles as a consequence of several dimensionless parameters.

2. Mathematical Formulation

Consider a three-dimensional incompressible steady OBF flow over a linearly stretching sheet with $U_w(x) = ax$. The fluid flow is considered in the domain $z > 0$ and the surface is associated in the x – y plane. With constant angular velocity Ω , the liquid is rotating about the z -axis. The mass and heat transfer components are inspected in the existence of concentration and thermal diffusions with the relaxation of mass and heat fluxes, respectively. In the presence of heat production or absorption, the boundary layer flow is also taken into account. Considering the above assumptions, the governing equations of the flow model can be written as follow (refs. [41–43])

$$\frac{\partial u}{\partial x} + \frac{\partial v}{\partial y} + \frac{\partial w}{\partial z} = 0 \tag{1}$$

$$\left. \begin{aligned} u \frac{\partial u}{\partial x} + v \frac{\partial u}{\partial y} + w \frac{\partial u}{\partial z} + \lambda_1 \left(\begin{aligned} &u^2 \frac{\partial^2 u}{\partial x^2} + v^2 \frac{\partial^2 u}{\partial y^2} + w^2 \frac{\partial^2 u}{\partial z^2} + 2uv \frac{\partial^2 u}{\partial x \partial y} + 2vw \frac{\partial^2 u}{\partial z \partial y} \\ &+ 2uw \frac{\partial^2 u}{\partial x \partial z} - 2\Omega \left(u \frac{\partial v}{\partial x} + v \frac{\partial v}{\partial y} + w \frac{\partial v}{\partial z} \right) + 2\Omega \left(v \frac{\partial u}{\partial x} - u \frac{\partial u}{\partial y} \right) \end{aligned} \right) - 2\Omega v = \end{aligned} \right\} \tag{2}$$

$$\left. \begin{aligned} v \left(\frac{\partial^2 u}{\partial z^2} + \lambda_2 \left[u \frac{\partial^3 u}{\partial x \partial z^2} + v \frac{\partial^3 u}{\partial y \partial z^2} + w \frac{\partial^3 u}{\partial z^3} - \frac{\partial u}{\partial x} \frac{\partial^2 u}{\partial z^2} - \frac{\partial u}{\partial y} \frac{\partial^2 v}{\partial z^2} - \frac{\partial u}{\partial z} \frac{\partial^2 w}{\partial z^2} \right] \right) \\ u \frac{\partial v}{\partial x} + v \frac{\partial v}{\partial y} + w \frac{\partial v}{\partial z} + \lambda_1 \left(\begin{aligned} &u^2 \frac{\partial^2 v}{\partial x^2} + v^2 \frac{\partial^2 v}{\partial y^2} + w^2 \frac{\partial^2 v}{\partial z^2} + 2uv \frac{\partial^2 v}{\partial x \partial y} + 2vw \frac{\partial^2 v}{\partial z \partial y} \\ &+ 2uw \frac{\partial^2 v}{\partial x \partial z} + 2\Omega \left(u \frac{\partial u}{\partial x} + v \frac{\partial u}{\partial y} + w \frac{\partial u}{\partial z} \right) + 2\Omega \left(v \frac{\partial v}{\partial x} - u \frac{\partial v}{\partial y} \right) \end{aligned} \right) + 2\Omega u = \end{aligned} \right\} \tag{3}$$

$$v \left(\frac{\partial^2 v}{\partial z^2} + \lambda_2 \left[u \frac{\partial^3 v}{\partial x \partial z^2} + v \frac{\partial^3 v}{\partial y \partial z^2} + w \frac{\partial^3 v}{\partial z^3} - \frac{\partial v}{\partial x} \frac{\partial^2 u}{\partial z^2} - \frac{\partial v}{\partial y} \frac{\partial^2 v}{\partial z^2} - \frac{\partial v}{\partial z} \frac{\partial^2 w}{\partial z^2} \right] \right) \\ u \frac{\partial T}{\partial x} + v \frac{\partial T}{\partial y} + w \frac{\partial T}{\partial z} + \Omega_e \Gamma_e = \frac{k}{(\rho C_p)} \left(\frac{\partial^2 T}{\partial z^2} \right) + \frac{Q_0}{(\rho C_p)} (T - T_\infty) \tag{4}$$

$$\left. \begin{aligned} u \frac{\partial C}{\partial x} + v \frac{\partial C}{\partial y} + w \frac{\partial C}{\partial z} + \Omega_c \Gamma_c = D \left(\frac{\partial^2 C}{\partial z^2} \right) - \frac{\partial(V_T(C - C_\infty))}{\partial z} + \\ k_r \left[\Gamma_c \left(u \frac{\partial C}{\partial x} + v \frac{\partial C}{\partial y} + w \frac{\partial C}{\partial z} \right) + (C - C_\infty) \right] \end{aligned} \right\} \tag{5}$$

where

$$\left. \begin{aligned} \Omega_e = & u^2 \frac{\partial^2 T}{\partial x^2} + v^2 \frac{\partial^2 T}{\partial y^2} + w^2 \frac{\partial^2 T}{\partial z^2} + 2uv \frac{\partial^2 T}{\partial x \partial y} + 2vw \frac{\partial^2 T}{\partial z \partial y} + 2uw \frac{\partial^2 T}{\partial z \partial x} + \\ & \left(u \frac{\partial u}{\partial x} + v \frac{\partial u}{\partial y} + w \frac{\partial u}{\partial z} \right) \frac{\partial T}{\partial x} + \left(u \frac{\partial v}{\partial x} + v \frac{\partial v}{\partial y} + w \frac{\partial v}{\partial z} \right) \frac{\partial T}{\partial y} + \left(u \frac{\partial w}{\partial x} + v \frac{\partial w}{\partial y} + w \frac{\partial w}{\partial z} \right) \frac{\partial T}{\partial z} \end{aligned} \right\} \quad (6)$$

$$\left. \begin{aligned} \Omega_c = & u^2 \frac{\partial^2 C}{\partial x^2} + v^2 \frac{\partial^2 C}{\partial y^2} + w^2 \frac{\partial^2 C}{\partial z^2} + 2uv \frac{\partial^2 C}{\partial x \partial y} + 2vw \frac{\partial^2 C}{\partial z \partial y} + 2uw \frac{\partial^2 C}{\partial z \partial x} + \\ & \left(u \frac{\partial u}{\partial x} + v \frac{\partial u}{\partial y} + w \frac{\partial u}{\partial z} \right) \frac{\partial C}{\partial x} + \left(u \frac{\partial v}{\partial x} + v \frac{\partial v}{\partial y} + w \frac{\partial v}{\partial z} \right) \frac{\partial C}{\partial y} + \left(u \frac{\partial w}{\partial x} + v \frac{\partial w}{\partial y} + w \frac{\partial w}{\partial z} \right) \frac{\partial C}{\partial z} \end{aligned} \right\} \quad (7)$$

The thermophoretic velocity V_T can be defined in the form [44]

$$V_T = -\frac{k^* \nu}{T_r} \frac{\partial T}{\partial Z} \quad (8)$$

where k^* has values from 0.2 to 1.2 as specified by Batchelor and Shen [45] and it is well-defined by Talbot et al. [46] as

$$k^* = \frac{2C_s \left(\frac{\lambda_g}{\lambda_p} + C_t Kn \right) \left[1 + Kn \left(C_1 + C_2 e^{-\frac{C_3}{Kn}} \right) \right]}{(1 + 3C_m Kn) \left(1 + \frac{\lambda_g}{\lambda_p} + 2C_t Kn \right)}, \quad (9)$$

where the thermal conductivities of fluid and diffused particles are represented by λ_g and λ_p , and $C_t = 2.20, C_s = 1.147, C_m = 1.146, C_1 = 1.2, C_2 = 0.41$ and $C_3 = 0.88$.

The flow is subjected to the related boundary constraints (refs. [41–43])

$$\left. \begin{aligned} Z = 0 : & u = U_w(x) = ax, v = 0, w = 0, T = T_w, C = C_w, \\ Z \rightarrow \infty : & u \rightarrow 0, v \rightarrow 0, T \rightarrow T_\infty, C \rightarrow C_\infty \end{aligned} \right\} \quad (10)$$

Considering the following suitable transformations, the governing equations can be simplified into the dimensionless form (refs. [41–43])

$$\left. \begin{aligned} u = axf'(\eta), v = axg(\eta), w = -\sqrt{av}f(\eta), \eta = \sqrt{\frac{a}{\nu}}z, \\ \theta(\eta) = \frac{T-T_\infty}{T_w-T_\infty}, \chi(\eta) = \frac{C-C_\infty}{C_w-C_\infty}. \end{aligned} \right\} \quad (11)$$

Using the above similarity transformations, the continuity Equation (1) is satisfied identically. Furthermore, the remaining Equations (2)–(5) are reduced to the following equations

$$f''' + ff'' - f'^2 + 2\lambda g - 2\lambda\beta_1 fg' - \beta_1(f^2 f''' - 2ff'f'') + \beta_2(-ff'v + f''^2) = 0 \quad (12)$$

$$g'' + fg' - f'g - 2\lambda[f' + \beta_1(f'^2 - ff'' + g^2)] + \beta_1(2ff'g' - f^2g'') + \beta_2(f'g'' + f''g' - fg''' - gf''') = 0, \quad (13)$$

$$\theta'' + Prf\theta' - Pr\lambda_E(ff'\theta' + f^2\theta'') + PrQ\theta = 0 \quad (14)$$

$$\chi'' + Scf\chi' - \lambda_C Sc(ff'\chi' + f^2\chi'') + Sc\sigma\chi - Sc\sigma\lambda_C f\chi' + ScN_t(\chi\theta'' + \chi'\theta') = 0 \quad (15)$$

The corresponding boundary conditions are transformed as

$$\left. \begin{aligned} \eta = 0 : & f = 0, f' = 1, g = 0, \theta = 1, \chi = 1, \\ \eta \rightarrow \infty : & f' \rightarrow 0, g \rightarrow 0, f'' \rightarrow 0, \theta \rightarrow 0, \chi \rightarrow 0. \end{aligned} \right\} \quad (16)$$

where $\lambda = \frac{\Omega}{a}, \beta_1 = \lambda_1 a, \beta_2 = \lambda_2 a, Q = \frac{Q_0}{\rho a C_p}, \lambda_E = a\Gamma_e, \lambda_C = a\Gamma_c$

$$Sc \frac{\nu}{D}, Pr = \frac{\nu}{\alpha}, N_t = \frac{k^*(T_w - T_\infty)}{T_r}, \sigma = \frac{k_r}{a}$$

Numerical Procedure

It does not seem that achieving the numerical solution of the existing model, which is very non-linear in nature, is feasible. As a result, we use an efficient traditional RKF-45 approach combined with shooting methodology to analyse the flow model for the aforementioned coupled ODEs (12–15) as well as the boundary conditions, Equation (16), for various values of the governing parameters. It is vital to note that the convergence is not guaranteed, specifically if the missing initial values are incorrectly predicted. When one of the domain end points is at infinity, another conflict occurs due to the instability of boundary value problems. As a result, the most important step in this strategy is to choose the appropriate finite value of η_∞ . We hand-picked an appropriate finite value of η_∞ to satisfy the far field boundary conditions asymptotically. Once convergence was achieved, we used the RKF-45 method to integrate the resulting ordinary differential equations with the supplied set of parameters to find the desired solution. Finally, in order to meet the convergence condition, the procedure was repeated until the findings were accurate to the specified degree of precision of 10^{-6} level. The step size was selected as $\Delta\eta = 0.0001$ and, along with the comparative error tolerance to 10^{-6} , was well-organized for convergence criteria. The results for the $-f''(0)$ and $-\theta'(0)$ were compared to existing publications to verify the present technique (see Tables 1 and 2).

Table 1. An assessment $-f''(0)$ for some reduced cases.

β_1 .	0	0.2	0.4	0.6	0.8	1.2
Abel et al. [47]	0.999996	1.051948	1.101850	1.150163	1.196692	1.285257
Megahed [48]	0.999978	1.051945	1.101848	1.150160	1.196690	1.285253
Sadeghy et al. [49]	1.00000	1.05490	1.10084	1.15016	1.19872	-----
Mustafa et al. [50]	1.000000	1.051890	1.101903	1.150137	1.196711	1.285363
Khan et al. [42]	1.000000	1.051889	1.101903	1.150137	1.196711	1.285363
Present results	1.000000	1.051890	1.101903	1.150137	1.196711	1.285363

Table 2. An assessment $-\theta'(0)$ for some reduced cases.

Pr .	0.7	2.0	7.0
Khan and Pop [51]	0.4539	0.9113	1.8954
Wang [52]	0.4539	0.9114	1.8954
Gorla and Sidawi [53]	0.4539	0.9114	1.8954
Khan et al. [42]	0.454374	0.911155	1.822020
Present results	0.454369	0.911148	1.822015

3. Results and Discussion

The graphical effects of the physical dimensionless quantities on involved profiles are discussed in this section. The equations that reflect the stated flow are changed to ODEs by picking apt similarity variables. A numerical scheme (RKF-45) with a shooting scheme is used to clearly understand the behaviour of flow profiles, which are strategized and debated using graphs. Figure 1 shows the influence of λ on $f'(\eta)$. The rise in values of λ decays the $f'(\eta)$. Figure 2 shows the impact of λ on $g(\eta)$. The upsurge in values of λ reduces the $g(\eta)$. In physical terms, the λ is the ratio of stretching rate and rotation rate. The velocity in the x-direction is seen to decrease when the Ω around the z-axis increases as the λ values are increased. Due to this, both $f'(\eta)$ and $g(\eta)$ decrease. The impact of β_1 on $f'(\eta)$ is shown in Figure 3. The upward β_1 values decreases $f'(\eta)$. Physically, β_1 depends

on λ_1 . Thus, with the escalation in β_1 this also augments λ_1 , which offers extra resistance to the fluid motion which increases $f'(\eta)$. The influence of β_2 on $f'(\eta)$ is shown in Figure 4. The increasing values of β_2 improves $f'(\eta)$. Physically, β_2 depends on λ_2 . Thus, with the rise in β_2 , this also augments λ_2 , which offers an additional resistance to the fluid motion, which increases the $f'(\eta)$.

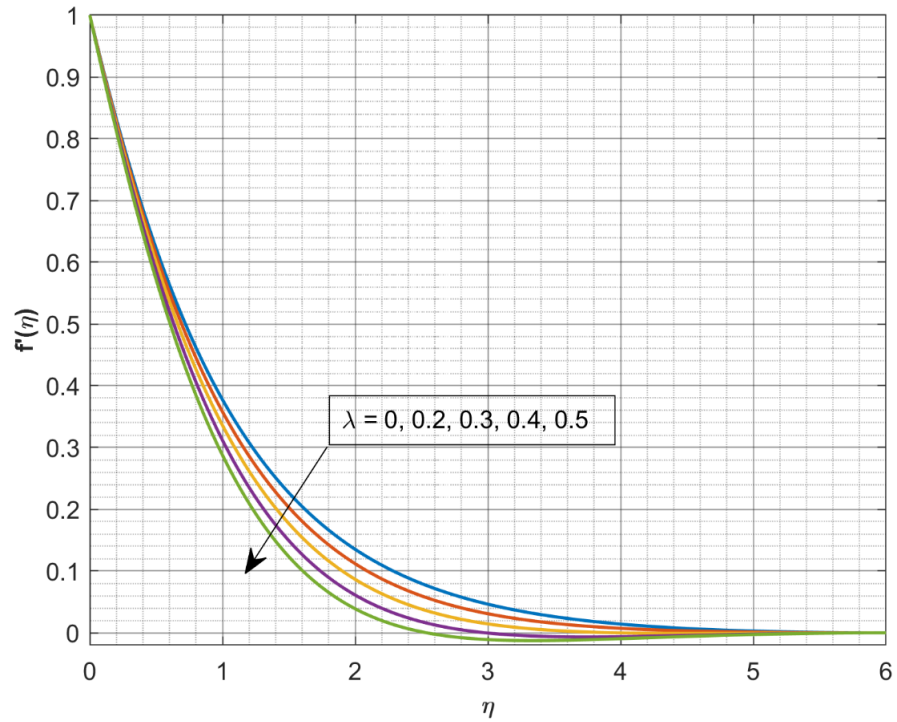


Figure 1. Influence of λ on $f'(\eta)$.

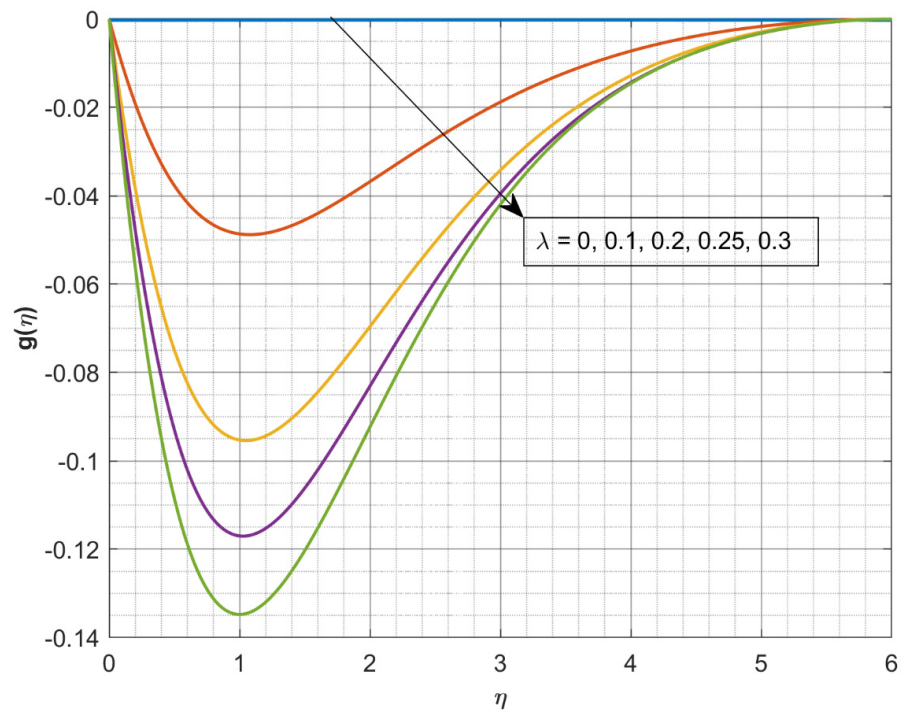


Figure 2. Influence of λ on $g(\eta)$.

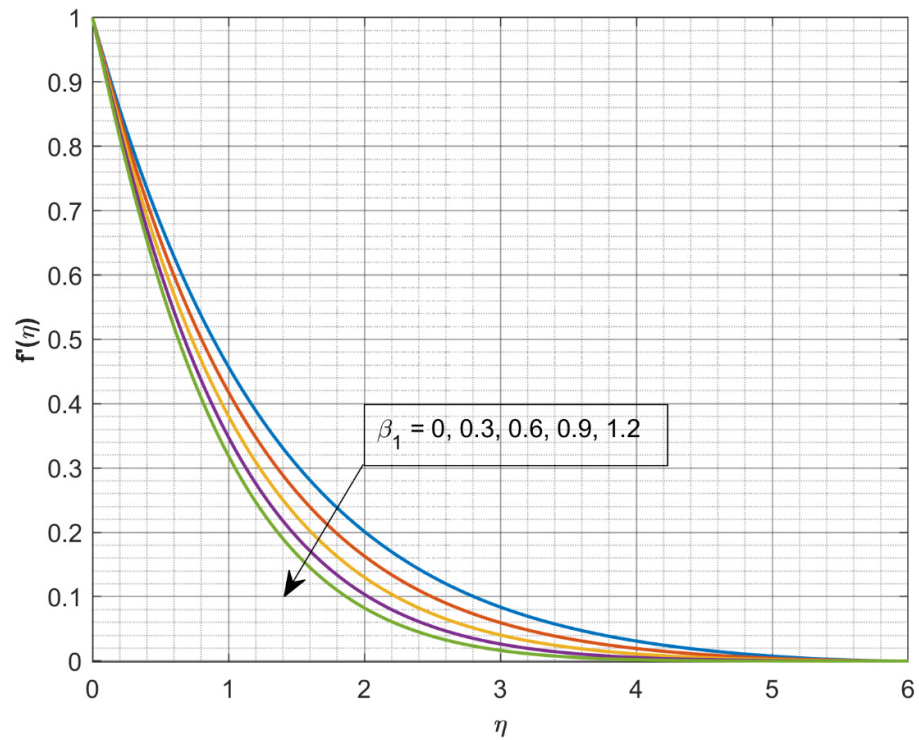


Figure 3. Influence of β_1 on $f'(\eta)$.

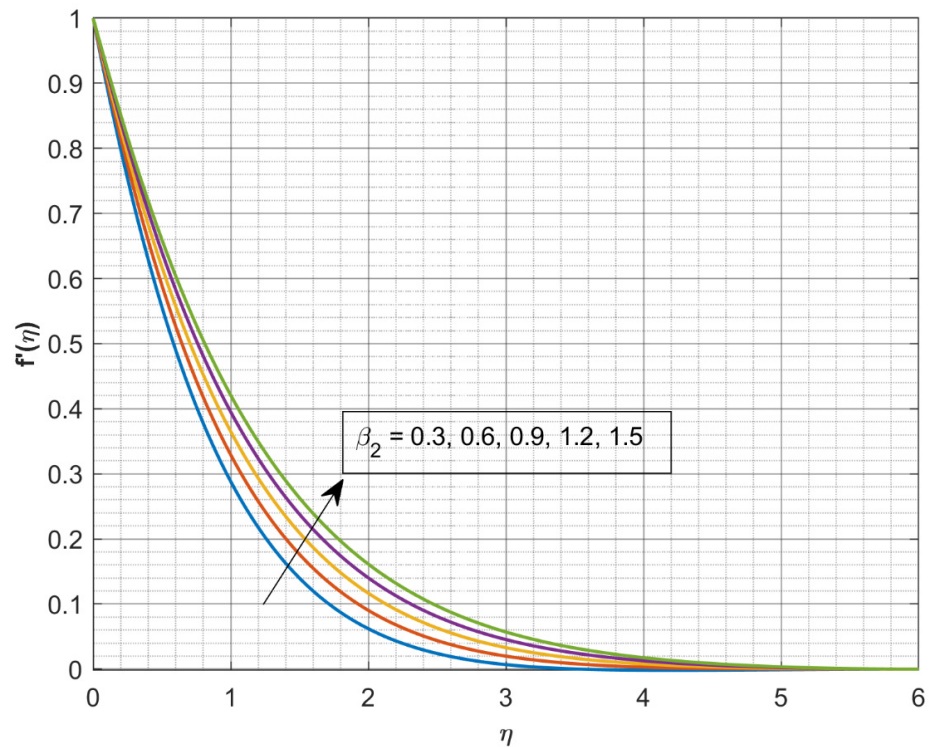


Figure 4. Influence of β_2 on $f'(\eta)$.

The consequence of Q on $\theta(\eta)$ is shown in Figure 5. The escalating values of Q improve $\theta(\eta)$. Internal heat absorption/generation either helps or degrades heat transport. Growth in the Q thickens the layer related to $\theta(\eta)$. The existence of the heat source restrictions in the flow state provides more excellent heat in this case. The presence of a heat source energizes the fluid. Consequently, as heat is consumed, the buoyancy force accelerates the

flow and improves the heat transfer. Figure 6 shows the effect of λ_E on $\theta(\eta)$. The rising values of λ_E reduces the $\theta(\eta)$. Physically, we may state that with higher values of the λ_E , the system exhibits a nonconducting characteristic that results in a narrowing of the thermal distribution. Furthermore when $\lambda_E = 0$, the temperature distribution in Fourier's law is more significant than in the Cattaneo–Christov heat flow model.

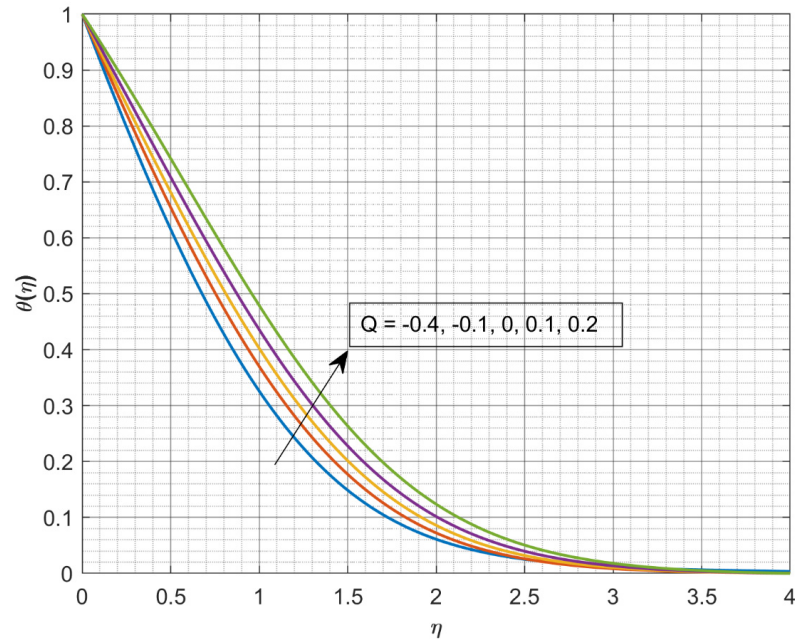


Figure 5. Influence of Q on $\theta(\eta)$.

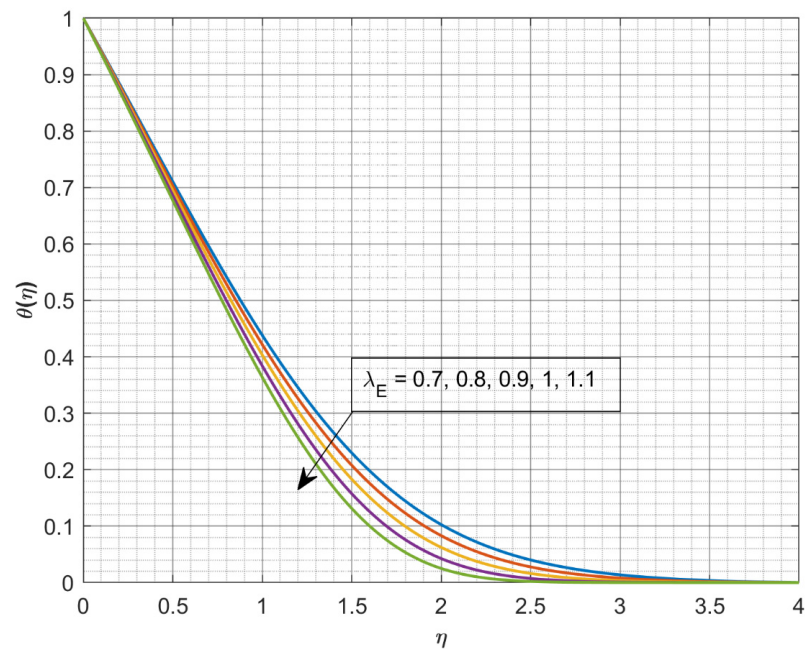


Figure 6. Influence of λ_E on $\theta(\eta)$.

Figure 7 displays the impact of Sc on $\chi(\eta)$. The increase in values of Sc drops $\chi(\eta)$. The smallest Sc correlates to the highest concentration of nanoparticles. For an upsurge in the Sc , there is a decay in the concentration field owing to mass diffusion. The effect of λ_C on $\chi(\eta)$ is shown in Figure 8. The escalating values of λ_C declines $\chi(\eta)$. In reality, a greater λ_C generates a weaker mass diffusivity, resulting in a narrower concentration distribution. A lower concentration field is produced by a higher value of λ_C . The effect of

σ on $\chi(\eta)$ is shown in Figure 9. The rising values of σ decreases $\chi(\eta)$. The fact that strong chemical reactions ($\sigma > 0$) have a tendency to reduce diffusion which is consequential in a decrease in chemical molecular diffusivity of the species concentration. Due to this retarded concentration of species, the $\chi_1(\eta)$ is decreased. Figure 10 portrays the impact of N_t on $\chi(\eta)$. The growing values of N_t upsurges $\chi(\eta)$. The growing values of N_t declines $\chi(\eta)$. When the thermophoresis parameter is superior, then the thermophoretic force increases, which pushes more particles nearer to the surface for a greater temperature differential, the concentration profiles on the cold surface are reduced as temperature ratios are raised.

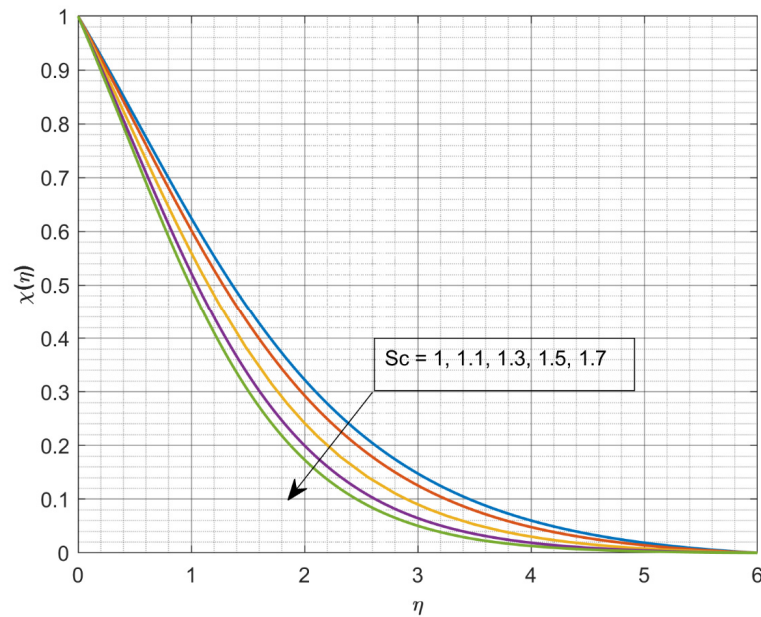


Figure 7. Influence of Sc on $\chi(\eta)$.

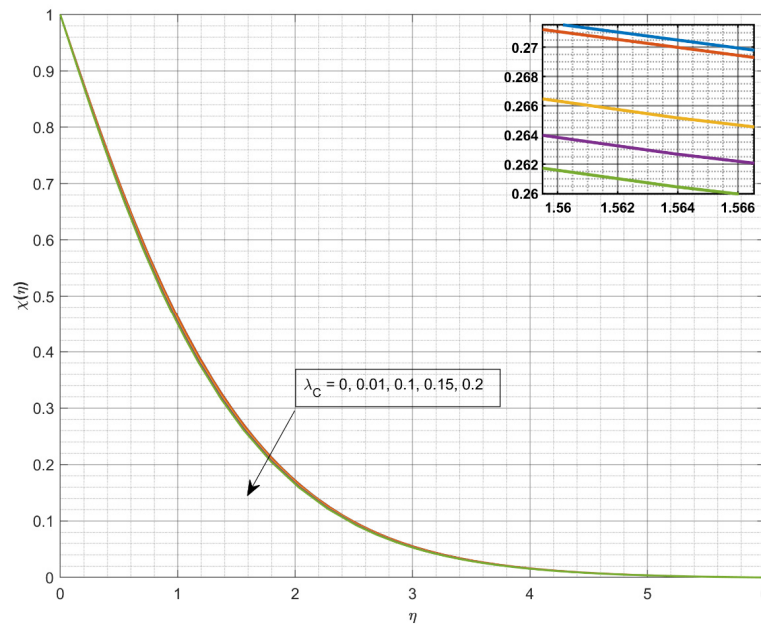


Figure 8. Influence of λ_C on $\chi(\eta)$.

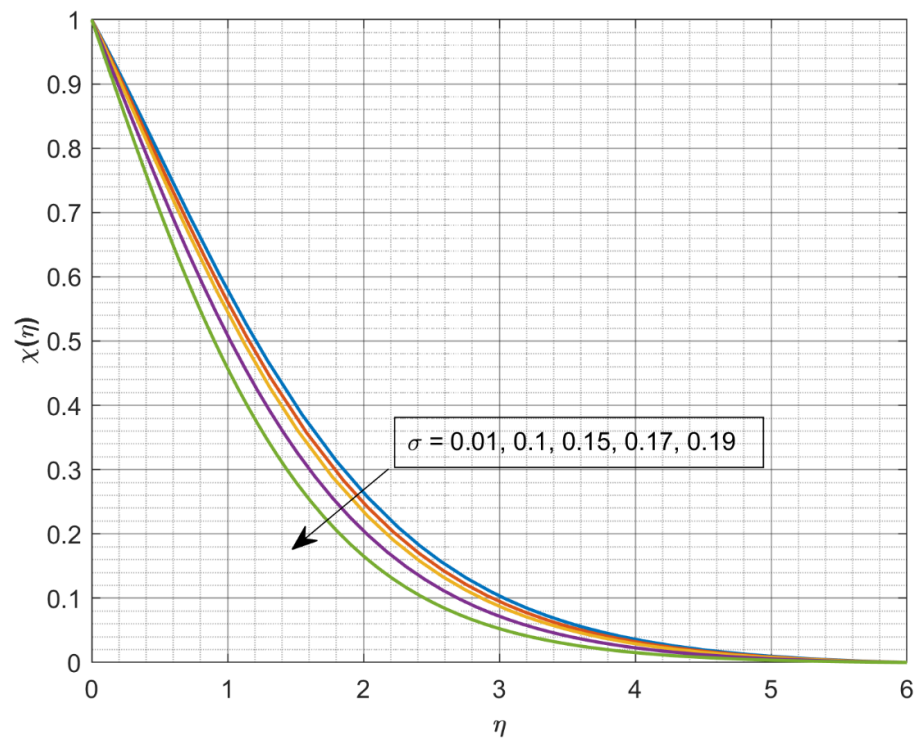


Figure 9. Influence of σ on $\chi(\eta)$.

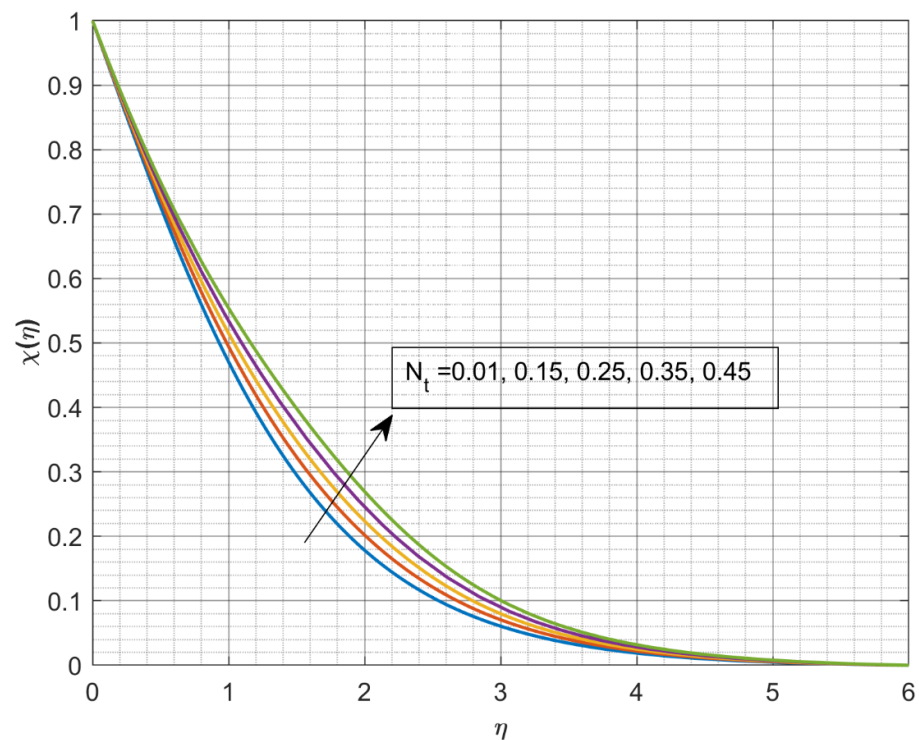


Figure 10. Influence of N_i on $\chi(\eta)$.

Table 3 portrays the numerical values of f'' with respect to pertinent varied parameters. The upsurge in the values of λ and β_2 reduces f'' , but the contrary tendency is detected for upward β_1 values. The numerical values of θ' with respect to pertinent varied parameters are shown in Table 4. The escalation in the values of λ and β_2 declines θ' , but the inverse trend is detected for the upward values of Q, β_1 , and λ_E . The numerical value of χ' with

respect to pertinent varied parameters is presented in Table 5. The escalation in Sc, σ , and N_t values declines χ' , but the reverse trend is detected for upward values of λ_C .

Table 3. The numerical values of f'' with respect to pertinent varied parameters.

λ	β_1	β_2	f''
0.2	0.8	1.1	-0.8484
0			-0.8395
0.1			-0.8418
0.11			-0.8422
0.12			-0.8427
	0.1		-0.7431
	0.15		-0.7508
	0.2		-0.7585
		0.1	-1.1745
		0.13	-1.1578
		0.15	-1.1593
		0.18	-1.6316

Table 4. The numerical values of θ' with respect to pertinent varied parameters.

λ	β_1	β_2	Q	λ_E	θ'
0.2	0.8	1.1	0.5	0.7	-0.1544
0					-0.1652
0.1					-0.1625
0.11					-0.1619
0.12					-0.1615
	0.1				-0.2587
	0.13				-0.2537
	0.15				-0.2504
	0.18				-0.2455
		0.1			0.0022
		0.13			-0.0045
		0.15			-0.0089
		0.18			-0.0153
			0.1		-0.5847
			0.2		-0.4995
			0.3		-0.4028
			0.4		-0.2902
				0.1	-0.1371
				0.2	-0.1331
				0.3	-0.1307
				0.4	-0.1306

Table 5. The numerical values of χ' with respect to pertinent varied parameters.

Sc	λ_C	σ	N_t	χ'
1.2	0.2	0.01	0.01	−0.6562
0.8				−0.5464
0.9				−0.574
1				−0.6016
1.1				−0.6276
	0.1			−0.671
	0.13			−0.6665
	0.15			−0.6636
	0.18			−0.6592
		0.1		−0.569
		0.13		−0.5379
		0.15		−0.5166
		0.18		−0.4834
			0.1	−0.6498
			0.13	−0.6477
			0.15	−0.6464
			0.18	−0.6445

4. Conclusions

The OBF flow analysis, in combination with mass and heat transfer initiated by an SS is utilized in the polymer industry and numerous industrial activities such as glass blowing and metallic sheet cooling. In the context of these applications, the current research explores the flow of Oldroyd-B liquid on a stretching sheet by considering Cattaneo–Christov double diffusion and heat source/sink. TPD is also considered in the modelling, and it is one of the most fundamental mechanisms for carrying microscopic particles over a thermal gradient, which is crucial in electronics and aeronautics. The equations that represent the indicated flow are changed to ODEs by electing relevant similarity variables. The ODEs are then solved using RKF-45 and shooting schemes. The behaviour of dimensionless parameters on dimensionless velocity, concentration, and temperature profiles are analyzed graphically. The following are the key findings of the present study:

- ❖ The rise in values of λ declines $f'(\eta)$ and $g(\eta)$.
- ❖ The increasing values of β_1 declines $f'(\eta)$, but a converse trend is seen for enhanced β_2 values.
- ❖ The rising values of Q improve $\theta(\eta)$.
- ❖ The rising values of λ_E reduces $\theta(\eta)$.
- ❖ The escalating values of λ_C and Sc declines $\chi(\eta)$.
- ❖ The increasing values of σ declines $\chi(\eta)$, but a reverse trend is seen for enhanced N_t values.
- ❖ The rise in values of λ and β_2 declines θ' , but the opposite trend is detected for upward values of Q, β_1 , and λ_E .
- ❖ The growth in values of Sc, σ , and N_t declines χ' , but the conflicting trend is detected for upward values of λ_C .

The future research could concentrate on the production of entropy as well as the effects of convective boundary conditions, Stefan blowing, and uniform/non-uniform heat sink/source on a variety of non-Newtonian fluid models with different nanoparticles' suspension in order to develop suitable mathematical models and simulate a variety of

hydrodynamic and thermal interface constraints under different conditions, and to develop a mathematical model for different nanoliquid flows.

Author Contributions: Conceptualization, B.C.P. and I.E.S.; methodology, B.C.P. and B.M.S.; software, B.J.G. and B.M.S.; validation, B.C.P. and I.E.S.; formal analysis, B.J.G.; investigation, B.M.S.; resources, I.E.S.; data curation, B.C.P.; writing—original draft preparation, B.J.G. and B.M.S.; writing—review and editing, I.E.S. and B.C.P.; visualization, B.J.G.; supervision, B.J.G., B.C.P. and I.E.S.; project administration, I.E.S. All authors have read and agreed to the published version of the manuscript.

Funding: This research received no external funding.

Conflicts of Interest: The authors declare no conflict of interest.

Nomenclature

(u, v, w)	velocity components
(x, y, z)	directions
ρ	density
μ	dynamic viscosity
λ_1	relaxation time
T_∞	ambient temperature
Γ_c	relaxation time for mass flux
k_r	reaction rate
D	diffusion coefficient
ν	kinematic viscosity
$Q = \frac{Q_0}{\rho a C_p}$	heat source/sink parameter
C_w	wall concentration
V_T	thermophoretic velocity
η	similarity variable
$\chi(\eta)$	dimensionless concentration profile.
$\lambda = \frac{\Omega}{a}$	rotation parameter
$\lambda_E = a\Gamma_e$	relaxation time parameter of temperature
$Sc = \frac{\nu}{D}$	Schmidt number
$N_t = \frac{k^*(T_w - T_\infty)}{T_r}$	thermophoretic parameter
a	positive constant
Ω	angular velocity
λ_2	retardation time
C_p	specific heat
k	thermal conductivity
C	concentration
$\beta_2 = \lambda_2 a$	Deborah number for retardation time
Q_0	heat source/sink coefficient
T	temperature
T_w	wall temperature
k^*	thermophoretic coefficient
T_r	reference temperature
C_∞	ambient concentration
$f(\eta), g'(\eta)$	dimensionless velocity profiles
$\theta(\eta)$	dimensionless thermal profile
Γ_e	relaxation time for heat flux
$\beta_1 = \lambda_1 a$	Deborah number for relaxation time
$\lambda_C = a\Gamma_c$	relaxation time parameter of concentration
$Pr = \frac{\nu}{\alpha}$	Prandtl number
$\sigma = \frac{k_r}{a}$	chemical reaction rate parameter

References

1. Irfan, M.; Khan, M.; Khan, W.; Alghamdi, M.; Ullah, M.Z. Influence of thermal-solutal stratifications and thermal aspects of non-linear radiation in stagnation point Oldroyd-B nanofluid flow. *Int. Commun. Heat Mass Transf.* **2020**, *116*, 104636. [[CrossRef](#)]
2. Reddy, G.K.; Yarrakula, K.; Raju, C.S.K.; Rahbari, A. Mixed convection analysis of variable heat source/sink on MHD Maxwell, Jeffrey, and Oldroyd-B nanofluids over a cone with convective conditions using Buongiorno's model. *J. Therm. Anal. Calorim.* **2018**, *132*, 1995–2002. [[CrossRef](#)]
3. Almakki, M.; Nandy, S.K.; Mondal, S.; Sibanda, P.; Sibanda, D. A model for entropy generation in stagnation-point flow of non-Newtonian Jeffrey, Maxwell, and Oldroyd-B nanofluids. *Heat Transf.-Asian Res.* **2019**, *48*, 24–41. [[CrossRef](#)]
4. Ramzan, M.; Howari, F.; Chung, J.D.; Kadry, S.; Chu, Y.-M. Irreversibility minimization analysis of ferromagnetic Oldroyd-B nanofluid flow under the influence of a magnetic dipole. *Sci. Rep.* **2021**, *11*, 1–19. [[CrossRef](#)]
5. Sarada, K.; Gowda, R.; Sarris, I.; Kumar, R.; Prasannakumara, B. Effect of Magneto hydrodynamics on Heat Transfer Behaviour of a Non-Newtonian Fluid Flow over a Stretching Sheet under Local Thermal Non-Equilibrium Condition. *Fluids* **2021**, *6*, 264. [[CrossRef](#)]
6. Hayat, T.; Qayyum, S.; Shehzad, S.A.; Alsaedi, A. Chemical reaction and heat generation/absorption aspects in flow of Walters-B nanofluid with Cattaneo-Christov double-diffusion. *Results Phys.* **2017**, *7*, 4145–4152. [[CrossRef](#)]
7. Gireesha, B.J.; Shankaralingappa, B.M.; Prasannakumar, B.C.; Nagaraja, B. MHD flow and melting heat transfer of dusty Casson fluid over a stretching sheet with Cattaneo-Christov heat flux model. *Int. J. Ambient. Energy* **2020**, 1–9. [[CrossRef](#)]
8. Sowmya, G.; Saleh, B.; Gowda, R.J.P.; Kumar, R.N.; Radhika, M. Analysis of radiative nonlinear heat transfer in a convective flow of dusty fluid by capitalizing a non-Fourier heat flux model. *Proc. Inst. Mech. Eng. Part E J. Process. Mech. Eng.* **2021**, 095440892111041192. [[CrossRef](#)]
9. Prasannakumara, B. Numerical simulation of heat transport in Maxwell nanofluid flow over a stretching sheet considering magnetic dipole effect. *Partial. Differ. Equ. Appl. Math.* **2021**, *4*, 100064. [[CrossRef](#)]
10. Gowda, R.J.P.; Rauf, A.; Kumar, R.N.; Prasannakumara, B.C.; Shehzad, S.A. Slip flow of Casson-Maxwell nanofluid confined through stretchable disks. *Indian J. Phys.* **2021**, 1–9. [[CrossRef](#)]
11. Hayat, T.; Qayyum, S.; Alsaedi, A.; Ahmad, B. Magneto hydrodynamic (MHD) nonlinear convective flow of Walters-B nanofluid over a nonlinear stretching sheet with variable thickness. *Int. J. Heat Mass Transf.* **2017**, *110*, 506–514. [[CrossRef](#)]
12. Prasannakumara, B.C. Assessment of the local thermal non-equilibrium condition for nanofluid flow through porous media: A comparative analysis. *Indian J. Phys.* **2021**, 1–9. [[CrossRef](#)]
13. Christopher, A.J.; Magesh, N.; Gowda, R.J.P.; Kumar, R.N.; Kumar, R.S.V. Hybrid nanofluid flow over a stretched cylinder with the impact of homogeneous-heterogeneous reactions and Cattaneo-Christov heat flux: Series solution and numerical simulation. *Heat Transf.* **2021**, *50*, 3800–3821. [[CrossRef](#)]
14. Gowda, R.J.P.; Jyothi, A.M.; Kumar, R.N.; Prasannakumara, B.C.; Sarris, I.E. Convective Flow of Second Grade Fluid Over a Curved Stretching Sheet with Dufour and Soret Effects. *Int. J. Appl. Comput. Math.* **2021**, *7*, 1–16. [[CrossRef](#)]
15. Alhadhrami, A.; Vishalakshi, C.; Prasanna, B.; Sreenivasa, B.; Alzahrani, H.A.; Gowda, R.P.; Kumar, R.N. Numerical simulation of local thermal non-equilibrium effects on the flow and heat transfer of non-Newtonian Casson fluid in a porous media. *Case Stud. Therm. Eng.* **2021**, *28*, 101483. [[CrossRef](#)]
16. Ali, B.; Hussain, S.; Shafiq, M.; Habib, D.; Rasool, G. Analyzing the interaction of hybrid base liquid $C_2H_6O_2-H_2O$ with hybrid nano-material Ag-MoS₂ for unsteady rotational flow referred to an elongated surface using modified Buongiorno's model: FEM simulation. *Math. Comput. Simul.* **2021**, *190*, 57–74. [[CrossRef](#)]
17. Ali, B.; Naqvi, R.A.; Hussain, D.; Aldossary, O.M.; Hussain, S. Magnetic Rotating Flow of a Hybrid Nano-Materials Ag-MoS₂ and Go-MoS₂ in $C_2H_6O_2-H_2O$ Hybrid Base Fluid over an Extending Surface Involving Activation Energy: FE Simulation. *Mathematics* **2020**, *8*, 1730. [[CrossRef](#)]
18. Ali, B.; Shafiq, A.; Siddique, I.; Al-Mdallal, Q.; Jarad, F. Significance of suction/injection, gravity modulation, thermal radiation, and magneto hydrodynamic on dynamics of micropolar fluid subject to an inclined sheet via finite element approach. *Case Stud. Therm. Eng.* **2021**, *28*, 101537. [[CrossRef](#)]
19. Ali, B.; Thumma, T.; Habib, D.; Salamat, N.; Riaz, S. Finite element analysis on transient MHD 3D rotating flow of Maxwell and tangent hyperbolic nanofluid past a bidirectional stretching sheet with Cattaneo Christov heat flux model. *Therm. Sci. Eng. Prog.* **2021**, 101089. [[CrossRef](#)]
20. Ali, B.; Siddique, I.; Ahmadian, A.; Senu, N.; Ali, L.; Haider, A. Significance of Lorentz and Coriolis forces on dynamics of water based silver tiny particles via finite element simulation. *Ain Shams Eng. J.* **2021**. [[CrossRef](#)]
21. Iasiello, M.; Vafai, K.; Andreozzi, A.; Bianco, N. Hypo- and hyperthermia effects on ldl deposition in a curved artery. *Comput. Therm. Sci. Int. J.* **2019**, *11*, 95–103. [[CrossRef](#)]
22. Iasiello, M.; Vafai, K.; Andreozzi, A.; Bianco, N.; Tavakkoli, F. Effects of External and Internal Hyperthermia on LDL Transport and Accumulation Within an Arterial Wall in the Presence of a Stenosis. *Ann. Biomed. Eng.* **2015**, *43*, 1585–1599. [[CrossRef](#)]
23. Iasiello, M.; Vafai, K.; Andreozzi, A.; Bianco, N. Low-density lipoprotein transport through an arterial wall under hyperthermia and hypertension conditions—An analytical solution. *J. Biomech.* **2016**, *49*, 193–204. [[CrossRef](#)]
24. RamReddy, C.; Murthy, P.; Chamkha, A.J.; Rashad, A. Soret effect on mixed convection flow in a nanofluid under convective boundary condition. *Int. J. Heat Mass Transf.* **2013**, *64*, 384–392. [[CrossRef](#)]

25. Ho, C.; Chen, D.-S.; Yan, W.-M.; Mahian, O. Buoyancy-driven flow of nanofluids in a cavity considering the Ludwig–Soret effect and sedimentation: Numerical study and experimental validation. *Int. J. Heat Mass Transf.* **2014**, *77*, 684–694. [[CrossRef](#)]
26. Kim, J.; Kang, Y.T.; Choi, C.K. Soret and Dufour effects on convective instabilities in binary nanofluids for absorption application. *Int. J. Refrig.* **2007**, *30*, 323–328. [[CrossRef](#)]
27. Manjunatha, P.; Gowda, R.P.; Kumar, R.N.; Suresha, S.; Sarwe, D.U. Numerical simulation of carbon nanotubes nanofluid flow over vertically moving disk with rotation. *Partial. Differ. Equ. Appl. Math.* **2021**, *4*, 100124. [[CrossRef](#)]
28. Gkountas, A.A.; Benos, L.T.; Sofiadis, G.N.; Sarris, I.E. A printed-circuit heat exchanger consideration by exploiting an Al₂O₃-water nanofluid: Effect of the nanoparticles interfacial layer on heat transfer. *Therm. Sci. Eng. Prog.* **2021**, *22*, 100818. [[CrossRef](#)]
29. Wang, F.; Asjad, M.I.; Zahid, M.; Iqbal, A.; Ahmad, H.; Alsulami, M. Unsteady thermal transport flow of Casson nanofluids with generalized Mittag–Leffler kernel of Prabhakar’s type. *J. Mater. Res. Technol.* **2021**, *14*, 1292–1300. [[CrossRef](#)]
30. Kumar, R.N.; Mallikarjuna, H.B.; Tigalappa, N.; Gowda, R.J.P.; Sarwe, D.U. Carbon nanotubes suspended dusty nanofluid flow over stretching porous rotating disk with non-uniform heat source/sink. *Int. J. Comput. Methods Eng. Sci. Mech.* **2021**, 1–10. [[CrossRef](#)]
31. Shehzad, S.A.; Mabood, F.; Rauf, A.; Tlili, I. Forced convective Maxwell fluid flow through rotating disk under the thermo-phoretic particles motion. *Int. Commun. Heat Mass Transf.* **2020**, *116*, 104693. [[CrossRef](#)]
32. Kumar, R.N.; Jyothi, A.; Alhumade, H.; Gowda, R.P.; Alam, M.M.; Ahmad, I.; Gorji, M.; Prasannakumara, B. Impact of magnetic dipole on thermophoretic particle deposition in the flow of Maxwell fluid over a stretching sheet. *J. Mol. Liq.* **2021**, *334*, 116494. [[CrossRef](#)]
33. Kumar, R.N.; Gowda, R.J.P.; Madhukesh, J.K.; Prasannakumara, B.C.; Ramesh, G.K. Impact of thermophoretic particle deposition on heat and mass transfer across the dynamics of Casson fluid flow over a moving thin needle. *Phys. Scr.* **2021**, *96*, 075210. [[CrossRef](#)]
34. Chen, S.-B.; Shahmir, N.; Ramzan, M.; Sun, Y.-L.; Aly, A.A.; Malik, M. Thermophoretic particle deposition in the flow of dual stratified Casson fluid with magnetic dipole and generalized Fourier’s and Fick’s laws. *Case Stud. Therm. Eng.* **2021**, *26*, 101186. [[CrossRef](#)]
35. Alhadhrami, A.; Alzahrani, H.A.; Kumar, R.N.; Gowda, R.P.; Sarada, K.; Prasanna, B.; Madhukesh, J.; Madhukeshwara, N. Impact of thermophoretic particle deposition on Glauert wall jet slip flow of nanofluid. *Case Stud. Therm. Eng.* **2021**, *28*, 101404. [[CrossRef](#)]
36. Zhang, Y.; Yuan, B.; Bai, Y.; Cao, Y.; Shen, Y. Unsteady Cattaneo–Christov double diffusion of Oldroyd-B fluid thin film with relaxation-retardation viscous dissipation and relaxation chemical reaction. *Powder Technol.* **2018**, *338*, 975–982. [[CrossRef](#)]
37. Mburu, Z.M.; Nayak, M.K.; Mondal, S.; Sibanda, P. Impact of irreversibility ratio and entropy generation on three-dimensional Oldroyd-B fluid flow with relaxation–retardation viscous dissipation. *Indian J. Phys.* **2021**, 1–17. [[CrossRef](#)]
38. Khan, M.I.; Khan, S.A.; Hayat, T.; Qayyum, S.; Alsaedi, A. Entropy generation analysis in MHD flow of viscous fluid by a curved stretching surface with cubic autocatalysis chemical reaction. *Eur. Phys. J. Plus* **2020**, *135*, 249. [[CrossRef](#)]
39. Gowda, R.P.; Kumar, R.N.; Jyothi, A.; Prasannakumara, B.; Sarris, I. Impact of Binary Chemical Reaction and Activation Energy on Heat and Mass Transfer of Marangoni Driven Boundary Layer Flow of a Non-Newtonian Nanofluid. *Processes* **2021**, *9*, 702. [[CrossRef](#)]
40. Yusuf, T.; Mabood, F.; Prasannakumara, B.; Sarris, I. Magneto-Bioconvection Flow of Williamson Nanofluid over an Inclined Plate with Gyrotactic Microorganisms and Entropy Generation. *Fluids* **2021**, *6*, 109. [[CrossRef](#)]
41. Shehzad, S.A.; Alsaedi, A.; Hayat, T.; Alhuthali, M.S. Three-Dimensional Flow of an Oldroyd-B Fluid with Variable Thermal Conductivity and Heat Generation/Absorption. *PLoS ONE* **2013**, *8*, e78240. [[CrossRef](#)]
42. Khan, W.; Irfan, M.; Khan, M. An improved heat conduction and mass diffusion models for rotating flow of an Oldroyd-B fluid. *Results Phys.* **2017**, *7*, 3583–3589. [[CrossRef](#)]
43. Khan, M.I.; Rashid, S.; Hayat, T.; Ayub, M.; Alsaedi, A. Magnetic effects in rotating flow of an Oldroyd-B fluid with chemical reaction and convective surface. *Indian J. Phys.* **2019**, *94*, 1361–1367. [[CrossRef](#)]
44. Shehzad, S.; Alsaedi, A.; Hayat, T.; Alhuthali, M. Thermophoresis particle deposition in mixed convection three-dimensional radiative flow of an Oldroyd-B fluid. *J. Taiwan Inst. Chem. Eng.* **2014**, *45*, 787–794. [[CrossRef](#)]
45. Batchelor, G.; Shen, C. Thermophoretic deposition of particles in gas flowing over cold surfaces. *J. Colloid Interface Sci.* **1985**, *107*, 21–37. [[CrossRef](#)]
46. Talbot, L.; Cheng, R.K.; Schefer, R.W.; Willis, D.R. Thermophoresis of particles in a heated boundary layer. *J. Fluid Mech.* **1980**, *101*, 737–758. [[CrossRef](#)]
47. Abel, M.S.; Tawade, J.V.; Nandeppanavar, M.M. MHD flow and heat transfer for the upper-convected Maxwell fluid over a stretching sheet. *Meccanica* **2012**, *47*, 385–393. [[CrossRef](#)]
48. Megahed, A.M. Variable fluid properties and variable heat flux effects on the flow and heat transfer in a non-Newtonian Maxwell fluid over an unsteady stretching sheet with slip velocity. *Chin. Phys. B* **2013**, *22*, 484–489. [[CrossRef](#)]
49. Sadeghy, K.; Hajibeygi, H.; Taghavi, S.M. Stagnation-point flow of upper-convected Maxwell fluids. *Int. J. Non-Linear Mech.* **2006**, *41*, 1242–1247. [[CrossRef](#)]
50. Mustafa, M.; Hayat, T.; Alsaedi, A. Rotating flow of Maxwell fluid with variable thermal conductivity: An application to non-Fourier heat flux theory. *Int. J. Heat Mass Transf.* **2017**, *106*, 142–148. [[CrossRef](#)]

-
51. Khan, W.A.; Pop, I. Boundary-layer flow of a nanofluid past a stretching sheet. *Int. J. Heat Mass Transf.* **2010**, *53*, 2477–2483. [[CrossRef](#)]
 52. Wang, C.Y. Free Convection on a Vertical Stretching Surface. *ZAMM* **1989**, *69*, 418–420. [[CrossRef](#)]
 53. Gorla, R.S.R.; Sidawi, I. Free convection on a vertical stretching surface with suction and blowing. *Flow Turbul. Combust.* **1994**, *52*, 247–257. [[CrossRef](#)]